# SINGULAR AND NEARLY SINGULAR QUADRATURE IN ARBITRARY DIMENSIONS*

JING HU†, LUQIANG HE*, AND SHUYU SUN‡

**Abstract.** The accurate numerical evaluation of integrals with singular or nearly singular kernels remains a fundamental challenge in scientific computing, particularly as the spatial dimension increases. While existing approaches, including singularity extraction, adaptive element subdivision, and analytical integration schemes, have achieved considerable success in one and two dimensions, their extension to higher dimensions is often hindered by severe near-singular behaviour and the resulting numerical instabilities. In this work, we propose a systematic approach for the high-accuracy evaluation of singular integrals and nearly singular integrals in arbitrary dimensions, based on variable transformation techniques derived from the Gauss hypergeometric function. We further analyze the structure of singularities and near-singularities in both the Duffy domain and the physical Cartesian domain, and establish a unified treatment via the sinh transformation. A convergence analysis based on the Bernstein ellipse parameter reveals that the sinh transformation ($\beta = 1$) consistently outperforms alternative hypergeometric transformations ($\beta = 2, 3$), which introduce secondary near-singularities despite achieving formal cancellation. Numerical experiments in dimensions two through five, together with an analysis of quadrature-induced consistency errors in variational discretisations, demonstrate that the proposed approach achieves exponential convergence and substantially outperforms direct Gauss–Legendre quadrature. The method offers a practical and theoretically grounded framework for high-dimensional nearly singular integration with broad applicability in scientific computing.

**Key words.** Convergence analysis, Duffy transformation, Singular integrals, Nearly singular integrals, Variable transformation

**MSC codes.** 65D32, 65D30

arXiv:2607.12440v1 [cs.CE] 14 Jul 2026

## 1. Introduction.

The numerical evaluation of integrals with singular or nearly singular kernels is a recurring computational bottleneck across many areas of scientific computing. Such integrals form the mathematical foundation of boundary integral equation formulations for elliptic partial differential equations [66, 36], potential theory, and fast multipole methods [47, 6]. In physical modelling, they are ubiquitous in acoustic and electromagnetic scattering [15, 39, 54, 2, 35, 64], wave propagation [16], and elastostatics and fracture mechanics [3, 60, 28, 69, 23]. Furthermore, the need for accurate singular quadrature extends to domains as diverse as computational fluid dynamics [53], biomechanics [11], computer graphics and radiosity [50, 45], and mathematical finance [30, 59]. When the source point lies on or near the integration domain, the integrand develops a sharp peak or an algebraic singularity that renders standard Gaussian quadrature ineffective [51, 4, 17, 9]. In the weakly singular case, the integral diverges in the ordinary sense and requires specialised regularisation; in the nearly singular case, the integrand remains bounded but develops steep gradients that cannot be adequately resolved by a fixed quadrature rule [7, 29]. These computational difficulties become substantially more severe as the spatial dimension increases, since the singularity structure couples across multiple coordinate directions and the cost of tensor-product quadrature grows exponentially [44].

Over the past decades, a variety of techniques have been developed to address this challenge. Singularity subtraction and extraction methods [21, 32, 23] isolate and integrate the singular part analytically, leaving a regular remainder for numerical

*Submitted to the editors DATE.

†College of Civil Engineering, Tongji University, Shanghai, China (jhu@tongji.edu.cn, luqianghe@tongji.edu.cn). Corresponding author: Jing Hu.

‡School of Mathematical Science,Tongji University, Shanghai, China (suns@tongji.edu.cn).

quadrature. Singularity swapping techniques [5, 1] replace the singular kernel with a smoother one that shares the same integral. Continuation approaches [48, 38, 58] construct a smooth continuation of the integrand away from the singularity. Adaptive subdivision methods [14] refine the integration mesh near the singular region, while analytical and semi-analytical schemes [37, 46, 24, 43] exploit closed-form expressions where available. Gauss–Jacobi quadrature frameworks for singular and nearly singular integrals on domains with edges and corners have been developed by Tsalamengas [56, 57], and Montanelli and coworkers [40, 41] have extended near-singular quadrature to curved boundary elements. Among all these techniques, variable transformation methods, including the Duffy transformation [18, 42], the sinh transformation [33], exponential and polynomial transformations [65, 62], and sigmoidal transformations [67], have proven particularly effective, as they regularise the integrand by clustering quadrature points in regions of rapid variation via a nonlinear change of variables.

Despite the wealth of available transformations, two significant gaps remain. First, there is no systematic framework for comparing the convergence properties of different transformations applied to the same singularity structure, making it difficult for practitioners to select an appropriate method for a given problem. The theory of exponential convergence for analytic functions provides a rigorous tool for such comparisons: for an analytic integrand, the Gauss–Legendre quadrature error on $m$ points is bounded by $C\rho^{-2m}$, where $\rho = |z^* + \sqrt{(z^*)^2 - 1}|$ is the Bernstein ellipse parameter associated with the nearest complex singularity $z^*$ [55, 68, 61, 63]. Yet, this analysis has rarely been applied systematically to evaluate competing variable transformations. Consequently, the question of which methods are genuinely effective, alongside the theoretical justifications for their success, remains largely unresolved. Second, most existing treatments are confined to one or two dimensions [13, 33, 12], while higher-dimensional scenarios—which arise, for example, in boundary integral formulations involving volumetric body forces or in high-dimensional parametric problems—have received comparatively little attention. Notable exceptions include the work of Mousavi and Sukumar [42] which generalised the Duffy transformation to high-dimensional vertex singularities, Latypov [37] which derived closed-form expressions for four-dimensional singular and nearly singular double surface integrals, and Gu et al. [22] which developed an algorithm for nearly strong-singular integrals in three-dimensional boundary element analysis. Sparse grid methods [20] can mitigate the exponential growth of tensor-product quadrature but are not directly applicable to singular integrands. A general treatment of nearly singular integrals in arbitrary dimensions, supported by rigorous convergence analysis, remains absent from the literature. Motivated by these considerations, Hu et al. [25] recently proposed a unified framework based on the Duffy transformation for two-dimensional weakly singular and nearly singular integrals, providing a comparative analysis of different variable transformations. The present work extends this line of investigation to higher dimensions.

In this work, we make the following contributions. First, working within the isoparametric framework, we systematically analyse the structure of singularities and near-singularities by examining the asymptotic behaviour of the integrand in both the Duffy domain and the physical Cartesian domain. We show that the near-singular behaviour associated with each integration variable can be reduced to a canonical form, enabling a unified treatment via the Gauss hypergeometric transformation. Second, we provide a convergence analysis based on the Bernstein ellipse parameter in the complex plane, which explains why the sinh transformation (the $\beta = 1$ member of

the hypergeometric family) is uniquely effective; the transformations with $\beta = 2$ and $\beta = 3$ introduce secondary near-singularities through their Jacobians, thereby degrading convergence despite achieving formal algebraic cancellation in the denominator. Third, we present numerical experiments in dimensions two through five that corroborate the theoretical analysis and demonstrate the substantial improvement in convergence rate afforded by the sinh transformation. Finally, we discuss the implications of accurate quadrature for the consistency error in variational discretisations, illustrating how the quality of numerical integration directly affects the total error of numerical solutions through Strang's first lemma [52].

The remainder of the paper is organised as follows. Section 2 analyses the singularity and near-singularity structure and presents the regularisation strategies, with convergence results integrated into each subsection. Section 3 provides numerical experiments in dimensions two through five. Section 4 discusses the significance of accurate quadrature for variational discretisations. Section 5 analyses the computational complexity, and Section 6 concludes with a summary and outlook.

## 2. Structure and regularisation of singular and nearly singular integrals.

**2.1. Problem formulation.** We consider integrals defined over an $n$-dimensional domain. In practical computations, the physical domain is discretised using curved elements with general geometries. To evaluate integrals over such elements in a systematic manner, it is standard practice to map the physical domain onto a reference isoparametric domain $\mathbf{D} = [-1, 1]^n$, where quadrature rules are canonically defined. In the isoparametric setting, the same shape functions are used to interpolate both the geometry and the field variables. An important consequence of this construction is that the mapping from the physical domain to the reference domain is a polynomial of fixed degree. As a result, a Taylor expansion of the geometry truncated at the order of the shape functions is exact; higher-order geometric terms, which would otherwise complicate the analysis of the singularity structure, do not arise. This property substantially simplifies the asymptotic analysis that follows. For more complex integration domains, it suffices to first map the physical domain onto the isoparametric reference domain; the subsequent analysis then applies without modification.

With this motivation, we consider an integral on a $n$-dimensional isoparametric space:

$$I = \int_{\mathbf{D}} \frac{f(\mathbf{x})}{\|\mathbf{x} - \mathbf{x}_\mathrm{s}\|^\alpha} \, \mathrm{d}\mathbf{D}, \qquad \mathbf{D} \subset \mathbb{R}^n, \tag{2.1}$$

where $f(\mathbf{x})$ is smooth, $\alpha > 0$, and $\mathbf{x}_\mathrm{s}$ is the source point. Let $\mathbf{x}_0 \in \mathbf{D}$ be the point on $\mathbf{D}$ closest to $\mathbf{x}_\mathrm{s}$, and define $\mathbf{r}_0 = \mathbf{x}_0 - \mathbf{x}_\mathrm{s}$ (Figure 1a). Eq. (2.1) becomes

$$I = \int_{\mathbf{D}} \frac{f(\mathbf{x})}{\|\mathbf{r}_0 + \mathbf{x} - \mathbf{x}_0\|^\alpha} \, \mathrm{d}\mathbf{D}, \qquad \mathbf{D} \subset \mathbb{R}^n. \tag{2.2}$$

Two regimes are distinguished:

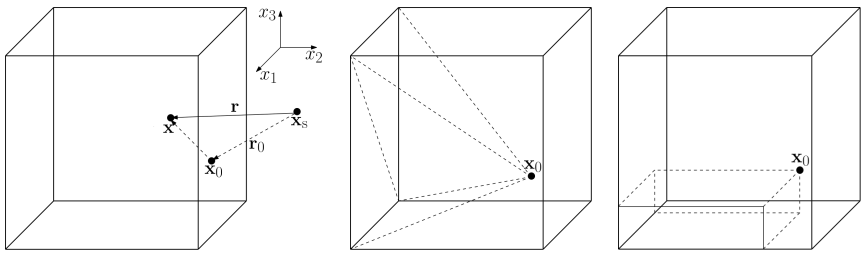
- Singular ($\mathbf{r}_0 = \mathbf{0}$): the source lies on the domain. The integral requires $\alpha < n$ for absolute convergence.
- Nearly singular ($0 < r_0 = \|\mathbf{r}_0\| \ll 1$): the source is close to the domain. The integrand is bounded but sharply peaked.

**2.2. Singular integrals: the Duffy transformation.** When $\mathbf{r}_0 = \mathbf{0}$, the integral reduces to

$$I = \int_{\mathbf{D}} \frac{f(\mathbf{x})}{\|\mathbf{x}-\mathbf{x}_0\|^\alpha}\,\mathrm{d}\mathbf{D}. \tag{2.3}$$

Let $\bar{\mathbf{x}}_0$ be the isoparametric coordinate of $\mathbf{x}_0$. Introduce the local coordinate $\boldsymbol{\xi} = \bar{\mathbf{x}} - \bar{\mathbf{x}}_0$ and partition $\mathbf{D} = [-1,1]^n$ into $m_1 = 2\cdot n!$ $n$-simplices, each sharing $\bar{\mathbf{x}}_0$ as a common vertex (Figure 1b). Eq. (2.2) becomes

$$I = \sum_{l=1}^{m_1} I_l = \sum_{l=1}^{m_1} \int_{\mathbf{D}_l} \frac{f(\mathbf{x})}{\|\mathbf{x}(\boldsymbol{\xi})-\mathbf{x}_0\|^\alpha}\,\mathrm{d}\mathbf{D}_l. \tag{2.4}$$




(a) Schematic of the problem (b) Duffy domain (c) Physical Cartesian domain

Fig. 1: Schematics of the domain partition for implementation in Duffy domain and physical Cartesian domain.

**2.2.1. Generalised Duffy transformation and cancellation.** On each simplex $\mathbf{D}_l$ with vertices $\{\bar{\mathbf{x}}_0, \bar{\mathbf{x}}_1, \ldots, \bar{\mathbf{x}}_n\}$, the generalised $n$-dimensional Duffy transformation maps $[0,1]^n$ onto $\mathbf{D}_l$:

$$\boldsymbol{\xi}^{(k)}(\boldsymbol{\theta}) = \sum_{j=1}^{n} \left(\prod_{i=1}^{j} \theta_i\right) \left(\boldsymbol{\xi}_j^{(k)} - \boldsymbol{\xi}_{j-1}^{(k)}\right), \qquad k = 1, \ldots, n, \tag{2.5}$$

where $\boldsymbol{\xi}_j^{(k)} = \bar{\mathbf{x}}_j^{(k)} - \bar{\mathbf{x}}_0^{(k)}$ and $\boldsymbol{\xi}_0^{(k)} \equiv 0$. The Jacobian is

$$J_{\text{Duffy}} = n! \prod_{j=1}^{n-1} \theta_j^{n-j} |S_l|, \tag{2.6}$$

where $|S_l|$ is the $n$-dimensional Lebesgue measure of $\mathbf{D}_l$.

To analyse the denominator, define the geometric Jacobian $\mathbf{S}^{(k)} = \partial\mathbf{x}/\partial\boldsymbol{\xi}^{(k)}|_{\bar{\mathbf{x}}_0}$ and the vector

$$\mathbf{P}_1(\theta_2, \ldots, \theta_n) = \sum_{k=1}^{n} \mathbf{S}^{(k)} \sum_{j=1}^{n} \Big(\prod_{i=2}^{j} \theta_i\Big) \big(\boldsymbol{\xi}_j^{(k)} - \boldsymbol{\xi}_{j-1}^{(k)}\big), \tag{2.7}$$

with the convention $\prod_{i=2}^{1}\theta_i \equiv 1$. In the isoparametric setting, a Taylor expansion of $\mathbf{x}$ in $\theta_1$ about $\mathbf{x}_0$ is exact at linear order:

$$\mathbf{x}(\boldsymbol{\xi}(\boldsymbol{\theta})) = \mathbf{x}_0 + \mathbf{P}_1(\theta_2,\ldots,\theta_n)\,\theta_1. \tag{2.8}$$

Hence the distance factorises as

$$r = \|\mathbf{x}-\mathbf{x}_0\| = \sqrt{c_2}\,\theta_1, \qquad c_2 = \mathbf{P}_1\cdot\mathbf{P}_1. \tag{2.9}$$

Substituting the Jacobian (2.6) and the distance (2.9) into the sub-integral (2.4) yields the cancellation that is the central mechanism of the Duffy method:

$$I_l = \int_{[0,1]^n} \frac{f(\mathbf{x})\,n!\prod_{j=2}^{n-1}\theta_j^{\,n-j}|S_l|}{c_2^{\alpha/2}\,\theta_1^{\alpha-n+1}} \prod_{j=1}^{n}\mathrm{d}\theta_j. \tag{2.10}$$

The Jacobian factor $\theta_1^{n-1}$ cancels against $\theta_1^{\alpha}$ from $r^{\alpha}$. The net exponent $p=\alpha-n+1$. The integral over $\theta_1\in[0,1]$ converges iff $p<1$, i.e. $\alpha<n$.

**2.2.2. Convergence of the Duffy-transformed singular integral.** We now quantify the convergence rate of Gauss–Legendre quadrature applied to Eq. (2.10). The analysis separates the radial ($\theta_1$) and angular ($\theta_2,\ldots,\theta_n$) directions.

**Radial direction.** For $\theta_1\in[0,1]$, the integrand behaves as $\theta_1^{-p}$ with $p=\alpha-n+1$. Three regimes arise:

1. $\alpha \le n-1$ **($p\le 0$):** The integrand is bounded or vanishes at $\theta_1=0$. Gauss–Legendre converges exponentially: $|E_1|\le C_1\rho_1^{-2m_1}$ with $\rho_1>1$.
2. $n-1<\alpha<n$ **($0<p<1$):** The integrand has an integrable algebraic singularity. Convergence is algebraic: $|E_1|\le C_1 m_1^{-2(n-\alpha)}$ [55].
3. $\alpha\ge n$ **($p\ge 1$):** The integral diverges.

In boundary integral applications, the most common case is $\alpha=n-1$ (i.e. weakly singular kernel), for which $p=0$ and radial convergence is exponential.

**Angular directions.** For each $\theta_j$ ($j\ge 2$), the integrand is analytic provided $c_2>0$. The convergence rate is governed by the nearest complex singularity of $c_2(\theta_2,\ldots,\theta_n)=0$. The Bernstein ellipse parameter is

$$\rho_j = \left|z_j^* + \sqrt{(z_j^*)^2-1}\right|, \qquad z_j^* = 2\theta_j^* - 1, \tag{2.11}$$

where $\theta_j^*$ is the nearest complex root of $c_2=0$. The per-dimension error is $|E_j|\le C_j\rho_j^{-2m_j}$.

**The angular factor $c_2$ and the effect of dimension.** To analyse $c_2$ uniformly across all $n$, define the geometric vectors

$$\mathbf{v}_j = \sum_{k=1}^{n}\mathbf{S}^{(k)}\big(\boldsymbol{\xi}_{j+1}^{(k)}-\boldsymbol{\xi}_j^{(k)}\big), \qquad j=0,1,\ldots,n-1, \tag{2.12}$$

with $\boldsymbol{\xi}_0^{(k)}\equiv 0$ so that $\mathbf{v}_0=\sum_k \mathbf{S}^{(k)}\boldsymbol{\xi}_1^{(k)}$. Substituting into Eq. (2.7) gives the expansion

$$\mathbf{P}_1(\theta_2,\ldots,\theta_n) = \mathbf{v}_0 + \theta_2\,\mathbf{v}_1 + \theta_2\theta_3\,\mathbf{v}_2 + \theta_2\theta_3\theta_4\,\mathbf{v}_3 + \cdots + \theta_2\theta_3\cdots\theta_n\,\mathbf{v}_{n-1}. \tag{2.13}$$

For $n=2$, the sum terminates at $\theta_2\mathbf{v}_1$, giving $\mathbf{P}_1=\mathbf{v}_0+\theta_2\mathbf{v}_1$., the sum contains two terms: $\mathbf{P}_1=\mathbf{v}_0+\theta_2\mathbf{v}_1$. In this case $c_2$ reduces to the quadratic form

$$c_2(\theta_2) = t_1\theta_2^2 + t_2\theta_2 + t_3, \qquad \theta_2\in[0,1], \tag{2.14}$$

with the coefficients

$$
\begin{aligned}
t_1 &= \Big(\sum_{k=1}^{n} \mathbf{S}^{(k)}\big(\boldsymbol{\xi}_2^{(k)} - \boldsymbol{\xi}_1^{(k)}\big)\Big) \cdot \Big(\sum_{k=1}^{n} \mathbf{S}^{(k)}\big(\boldsymbol{\xi}_2^{(k)} - \boldsymbol{\xi}_1^{(k)}\big)\Big), \\
t_2 &= 2\Big(\sum_{k=1}^{n} \mathbf{S}^{(k)}\big(\boldsymbol{\xi}_2^{(k)} - \boldsymbol{\xi}_1^{(k)}\big)\Big) \cdot \Big(\sum_{k=1}^{n} \mathbf{S}^{(k)}\big(\boldsymbol{\xi}_1^{(k)} - \boldsymbol{\xi}_0^{(k)}\big)\Big), \\
t_3 &= \Big(\sum_{k=1}^{n} \mathbf{S}^{(k)}\big(\boldsymbol{\xi}_1^{(k)} - \boldsymbol{\xi}_0^{(k)}\big)\Big) \cdot \Big(\sum_{k=1}^{n} \mathbf{S}^{(k)}\big(\boldsymbol{\xi}_1^{(k)} - \boldsymbol{\xi}_0^{(k)}\big)\Big).
\end{aligned}
\tag{2.15}
$$

A key observation from (2.13) is that for $n \geq 3$, the series includes terms coupling at least two angular variables (i.e. $\theta_2\theta_3\mathbf{v}_2$ and beyond). For general $n$, the $j$-th term couples the product of the first $j$ angular variables, with the final term $\theta_2 \cdots \theta_n \mathbf{v}_{n-1}$ coupling all $n-1$ angular variables simultaneously. Squaring $\mathbf{P}_1$ gives the general expression

$$
c_2 = \sum_{j=0}^{n-1} \|\mathbf{v}_j\|^2 \Big(\prod_{i=2}^{j+1} \theta_i\Big)^2 \; + \; 2 \sum_{0 \leq j < \ell \leq n-1} (\mathbf{v}_j \cdot \mathbf{v}_\ell) \Big(\prod_{i=2}^{j+1} \theta_i\Big)\Big(\prod_{i=2}^{\ell+1} \theta_i\Big).
\tag{2.16}
$$

For $n = 2$, the double sum reduces to the single term $(j, \ell) = (0, 1)$, and Eq. (2.16) reproduces the quadratic (2.14) with $t_1 = \|\mathbf{v}_1\|^2$, $t_2 = 2(\mathbf{v}_0 \cdot \mathbf{v}_1)$, and $t_3 = \|\mathbf{v}_0\|^2$. For $n \geq 3$, terms with $\ell - j \geq 2$ generate monomials such as $\theta_2\theta_3$ (from $j = 0, \ell = 2$) that couple distinct angular variables; the double sum cannot be expressed as a sum of univariate functions.

**Geometric obstruction for distorted simplices.** For a well-shaped simplex, $c_2$ is bounded away from zero; all $\rho_j$ are bounded away from unity; and Gauss–Legendre converges exponentially in every direction regardless of $n$. For a distorted simplex ($c_2 \approx 0$ for some angular values), the near-singular set

$$
\mathcal{M} = \{(\theta_2, \ldots, \theta_n) \in [0, 1]^{n-1} : c_2 \approx 0\}
\tag{2.17}
$$

is generically an $(n-2)$-dimensional manifold:

- $n = 2$: $\mathcal{M}$ is a point (dimension 0);
- $n = 3$: $\mathcal{M}$ is a curve (dimension 1);
- $n = 4$: $\mathcal{M}$ is a surface (dimension 2).

A tensor-product quadrature rule places nodes on a Cartesian grid in $[0, 1]^{n-1}$. Applying independent 1D nonlinear transformations to each angular variable can cluster nodes near any axis-aligned point (a 0-dimensional locus), but cannot cluster nodes around a manifold of dimension $\geq 1$ that is oblique to the coordinate axes. No separable change of variables can alter this, because separability preserves the Cartesian-product structure of the node set. The angular convergence therefore degrades for distorted simplices when $n > 2$. In summary, the Duffy transformation provides a valid method for singular integrals in any dimension $n$: the radial singularity is cancelled by the Jacobian when $\alpha < n$, and for well-shaped simplices all variables converge exponentially. For distorted simplices with $n > 2$, the angular convergence degrades because the $(n-2)$-dimensional near-singular manifold may not be well resolved by a tensor-product rule. This is a robustness limitation of Duffy transformation; adaptive simplex subdivision can mitigate it in practice [42].

**2.3. Nearly singular integrals: limitation of the Duffy domain.** We now return to the nearly singular case ($0 < r_0 \ll 1$). Applying the Duffy transformation (2.5) to Eq. (2.2) and using the orthogonality $\mathbf{r}_0 \cdot \mathbf{P}_1 = 0$ (since $\bar{\mathbf{x}}_0$ is the projection of $\mathbf{x}_s$ onto $\mathbf{D}$), we obtain

$$I_l = \int_{[0,1]^n} \frac{f(\mathbf{x})\, n! \prod_{j=1}^{n-1} \theta_j^{n-j} |S_l|}{(r_0^2 + c_2 \theta_1^2)^{\alpha/2}} \prod_{j=1}^{n} \mathrm{d}\theta_j. \tag{2.18}$$

Two critical differences from the singular case emerge. First, the denominator does not factorise: the Jacobian factor $\theta_1^{n-1}$ provides no cancellation when $r_0 > 0$. Second, both $\theta_1$ and the angular variables exhibit near-singular behaviour. The near-singularity in $\theta_1$ has the canonical form $(r_0^2 + c_2\theta_1^2)^{-\alpha/2}$, which is a 1D structure treatable with a 1D nonlinear transformation in any dimension. The angular near-singularity enters through $c_2^{-\alpha/2}$, exactly as in the singular case.

For $n = 2$, the angular variable is a single scalar $\theta_2$, and $c_2(\theta_2)$ is a quadratic. Duffy transformation followed by independent 1D sinh transformations on $\theta_1$ and $\theta_2$ completely regularises the integral. For $n > 2$, however, the angular variables $\theta_2, \ldots, \theta_n$ are coupled through $c_2$ (Eq. 2.16). The near-singular manifold $\mathcal{M} = \{c_2 \approx 0\}$ has dimension $n - 2 \geq 1$. As argued in Section 2.2, a tensor-product rule cannot resolve such a manifold. The Duffy-domain strategy therefore does not extend to $n > 2$ for nearly singular integrals. This geometric obstruction motivates the physical Cartesian domain treatment developed next.

**2.4. Nearly singular integrals: the physical-domain approach.** To overcome the geometric obstruction, we abandon the Duffy parametrisation and work directly in the physical (Cartesian) domain. The integration domain is subdivided into $2^n$ hyper-rectangles, each sharing a vertex at $\bar{\mathbf{x}}_0$ (Figure 1c). The integral becomes

$$I = \sum_{l=1}^{m_2} I_l = \sum_{l=1}^{m_2} \int_{a_1}^{b_1} \cdots \int_{a_n}^{b_n} \frac{f(\mathbf{x})}{\|\mathbf{r}_0 + \mathbf{x}(\boldsymbol{\xi}) - \mathbf{x}_0\|^{\alpha}} \, \mathrm{d}\boldsymbol{\xi}^{(1)} \cdots \mathrm{d}\boldsymbol{\xi}^{(n)}. \tag{2.19}$$

Singular integrals cannot be treated in this domain because the Duffy Jacobian is absent.

Expanding $\mathbf{x} = \mathbf{x}_0 + \sum_{k=1}^{n} \mathbf{S}^{(k)} \boldsymbol{\xi}^{(k)}$ and using $\mathbf{r}_0 \cdot \mathbf{S}^{(k)} = 0$,

$$I_l = \int_{a_1}^{b_1} \cdots \int_{a_n}^{b_n} \frac{f(\mathbf{x})}{\left(r_0^2 + \sum_{j=1}^{n} \sum_{k=1}^{n} \mathbf{S}^{(j)} \cdot \mathbf{S}^{(k)} \, \boldsymbol{\xi}^{(j)} \boldsymbol{\xi}^{(k)}\right)^{\alpha/2}} \, \mathrm{d}x_1 \cdots \mathrm{d}x_n. \tag{2.20}$$

Defining $c_k = \mathbf{S}^{(k)} \cdot \mathbf{S}^{(k)}$, the near-singular structure in each coordinate direction takes form

$$\frac{1}{d_0^2 + c_k (\boldsymbol{\xi}^{(k)})^2}. \tag{2.21}$$

where $d_0^2 = r_0^2 + \sum_{j \neq k} c_j (\boldsymbol{\xi}^{(j)})^2$ aggregates the squared distance $r_0^2$ and the diagonal contributions except for $c_k (\boldsymbol{\xi}^{(k)})^2$. The cross-coupling terms through $\mathbf{S}^{(j)} \mathbf{S}^{(k)}$ for $j \neq k$ are neglected under the assumption of an affine (or nearly affine) geometric mapping; see Remark 2.1. A direct transformation of this coupled structure compromises the separability of the integration variables, which prevents the use of tensor-product

multidimensional Gaussian quadrature. However, it can be seen that the sharpest near-singularity occurs when the contribution of the other variables to $d_0^2$ is minimal, since each diagonal term is non-negative. As a result, the above structure degenerates into

$$\frac{1}{r_0^2 + c_k(\boldsymbol{\xi}^{(k)})^2}. \tag{2.22}$$

At this point, the transformation to be performed is independent of the other variables, and the nearly singularity is effectively decoupled.

In summary, the physical-domain approach resolves the geometric obstruction identified in Section 2.3. By subdividing the domain into hyper-rectangles and expanding the geometry in Cartesian coordinates, the near-singularities align with the coordinate axes. Each direction then carries an independent 1D near-singularity of the canonical form $(r_0^2+c_k\xi_k^2)^{-\alpha/2}$, which can be treated by a 1D sinh transformation. This provides a robust method for nearly singular integrals in arbitrary dimension $n$. The price is that singular integrals cannot be treated in this domain, since the Duffy Jacobian which provides the cancellation of the $1/r^\alpha$ singularity is absent.

*Remark* 2.1 (Cross-terms in the physical domain). The derivation of (2.21) neglects the cross-terms $\mathbf{S}^{(j)}\cdot\mathbf{S}^{(k)}\boldsymbol{\xi}^{(j)}\boldsymbol{\xi}^{(k)}$ for $j \neq k$. This is equivalent to assuming that the isoparametric Jacobian matrix $[\mathbf{S}^{(k)}]$ is diagonal at $\bar{\mathbf{x}}_0$, i.e. the element edges are orthogonal at the projection point. For general curved or non-orthogonal elements, these cross-terms contribute additional coupling. A rigorous treatment requires either a coordinate diagonalisation or an estimate of the cross-term contribution, which we defer to future work.

**2.5. The sinh transformation and its competitors.** The canonical near-singular structure $(r_0^2 + c\,\xi^2)^{-\alpha/2}$ that appears in both the Duffy domain (for $\theta_1$ and, when $n = 2$, for $\theta_2$) and the physical Cartesian domain (for each $\xi^{(k)}$) motivates a unified treatment. We exploit the Jacobian of a nonlinear change of variables to eliminate or weaken the near-singular behaviour.

**2.5.1. The Gauss hypergeometric family.** For an integrand of the prototypical form

$$\frac{1}{\left(\sqrt{t_1(\theta+b)^2+d^2}\,\right)^{\beta}}, \qquad t_1, d > 0, \;\; b \leq 0, \tag{2.23}$$

the unified transformation is

$$\Theta(\theta) = d^{-\beta}\Big(-b\,{}_2F_1\Big(\frac{1}{2},\frac{\beta}{2};\frac{3}{2};-\frac{b^2t_1}{d^2}\Big) + (b+\theta)\,{}_2F_1\Big(\frac{1}{2},\frac{\beta}{2};\frac{3}{2};-\frac{t_1(b+\theta)^2}{d^2}\Big)\Big), \tag{2.24}$$

where ${}_2F_1$ is the Gauss hypergeometric function. The transformation requires an explicit inverse for use with Gauss–Legendre quadrature. Closed-form inverses exist only for $\beta = 1, 2, 3$, corresponding to the sinh, tangent, and algebraic transformations. For $b = 0$ (the case relevant to the canonical form), the inverse functions and their

Jacobians are

(2.25)
$$\theta(\Theta) = \begin{cases} \dfrac{d}{\sqrt{t_1}} \sinh\big(\sqrt{t_1}\,\Theta\big), & \beta = 1 \\ \dfrac{d}{\sqrt{t_1}} \tan\big(d\sqrt{t_1}\,\Theta\big), & \beta = 2 \\ \dfrac{d^3\Theta}{\sqrt{1 - t_1 d^4 \Theta^2}}, & \beta = 3, \end{cases} \qquad J(\Theta) = \begin{cases} d\cosh\big(\sqrt{t_1}\,\Theta\big), & \beta = 1 \\ d^2 \sec^2(d\sqrt{t_1}\,\Theta), & \beta = 2 \\ \dfrac{d^3}{(1 - t_1 d^4 \Theta^2)^{3/2}}, & \beta = 3. \end{cases}$$

When $\alpha = \beta$, the transformation achieves exact cancellation of the denominator, leaving only the smooth numerator and the Jacobian. It is therefore expected that matching $\beta$ to $\alpha$ yields optimal performance, however the convergence analysis below shows this intuition to be incorrect for $\beta = 2, 3$.

**2.5.2. Convergence of the sinh transformation ($\beta = 1$).** For an analytic integrand, the $m$-point Gauss–Legendre error is bounded by $C\rho^{-2m}$, where $\rho = |p_s + \sqrt{p_s^2 - 1}|$ is the Bernstein ellipse parameter associated with the nearest complex singularity $p_s$ of the transformed integrand [55, 68, 61, 63]. The singularities of $(r_0^2 + c\xi^2)^{-\alpha/2}$ lie at $\xi_s = \pm i r_0/\sqrt{c}$. Mapping to $p = 2\xi - 1 \in [-1, 1]$ gives $p_s = -1 \pm 2ir_0/\sqrt{c}$, with $\rho_0 = 1 + 2r_0/\sqrt{c} + O(r_0^2) \to 1$ as $r_0 \to 0$. Standard Gauss–Legendre therefore fails.

**Sinh transformation.** After applying the sinh transformation, the upper limit is

$$\Theta_1 = \frac{\operatorname{arcsinh}(\sqrt{c}/r_0)}{\sqrt{c}} \xrightarrow{r_0 \to 0} \frac{\ln(2\sqrt{c}/r_0)}{\sqrt{c}}. \tag{2.26}$$

The Jacobian $\cosh(\sqrt{c}\,\Theta)$ has its nearest singularity at $\Theta_s = i\pi/(2\sqrt{c})$. Mapping to the $p$-domain:

$$p_s^{(\beta=1)} = \frac{2\Theta_s}{\Theta_1} - 1 = \frac{i\pi}{\operatorname{arcsinh}(\sqrt{c}/r_0)} - 1. \tag{2.27}$$

The imaginary part approaches zero only at a logarithmic rate as $r_0 \to 0$. The Bernstein parameter therefore departs from unity slowly, preserving exponential convergence for practical $m$. The arcsinh function acts as a regulariser: it pushes complex singularities away from the real axis.

For $\alpha > 1$, the denominator retains a factor $\cosh^{\alpha}(\sqrt{c}\,\Theta)$, so cancellation is not exact. The logarithmic mechanism still ensures the transformed integrand is substantially smoother than the original, and the imaginary part of $p_s$ does not tend to zero.

**Tangent ($\beta = 2$) and algebraic ($\beta = 3$) transformations.** The analysis (detailed in Appendix A) shows that both transformations introduce new singularities through their Jacobians that map to the real axis after mapping to $[-1, 1]$, collapsing $\rho$ to unity. The quadrature error therefore decays arbitrarily slowly. Figure 2 compares the Bernstein ellipse parameter as a function of $r_0$ for all three transformations (with $c = 1$).

In summary, among the three closed-form members of the Gauss hypergeometric family, only the sinh transformation ($\beta = 1$) consistently improves convergence. The tangent ($\beta = 2$) and algebraic ($\beta = 3$) transformations introduce secondary near-singularities through their Jacobians; after domain mapping, the corresponding

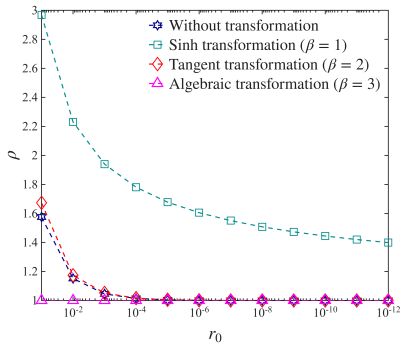



Fig. 2: Bernstein ellipse parameter of the three hypergeometric transformations as a function of $r_0$ (with $c = 1$). The sinh transformation ($\beta = 1$) approaches unity at the slowest rate.

Bernstein ellipse parameters collapse to unity, yielding arbitrarily slow convergence. The sinh transformation is therefore the unique effective member of the family, and it is the transformation employed throughout the remainder of this work.

**3. Numerical examples.** To verify the proposed framework, we present computational examples in dimensions two through five. In all cases, the sinh transformation ($\beta = 1$) is compared against direct Gauss–Legendre quadrature; for $n \geq 3$, we further compare it with the tangent ($\beta = 2$) and algebraic ($\beta = 3$) transformations. Benchmark values are obtained using a large number of Gauss points in the transformed domain. The error is $E = |I - I_{\text{num}}|$.

*Double integral ($n = 2$).* Consider

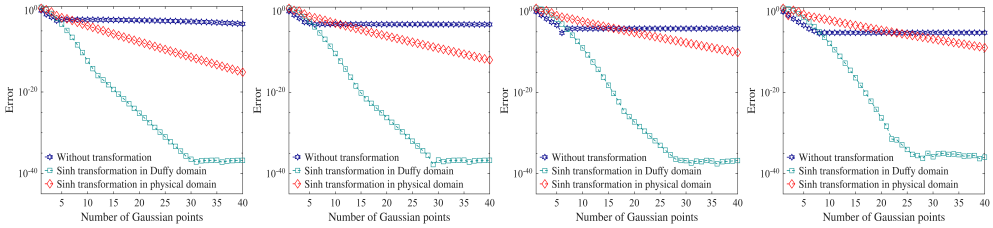
$$\iint_{[-1,1]^2} \frac{1}{\sqrt{(x-e_1)^2 + (y-e_2)^2 + c^2}} \, \mathrm{d}x \, \mathrm{d}y, \tag{3.1}$$

the 2D weakly singular kernel arising in boundary element formulations of the Laplace and Helmholtz equations [15, 49], heat conduction [10], Darcy flow [26], and fracture mechanics [8, 27]. Figure 3 shows results for $e_1 = e_2 = 0$ (source centred, top row) and $e_1, e_2$ close to the boundary (bottom row), both with and without the sinh transformation in the Duffy domain and physical (Cartesian) domain. Applying the sinh transformation in the Duffy domain yields better performance than in the physical domain, owing to additional regularisation from the Duffy Jacobian.

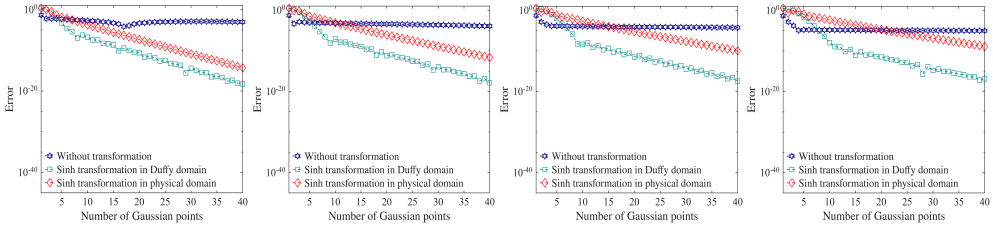
*Triple, quadruple, and quintuple integrals ($n = 3, 4, 5$).* To systematically evaluate the proposed framework in higher dimensions, we consider a sequence of $n$-dimensional volume integrals featuring the near-singular exponent $\alpha = n - 1$. This specific exponent corresponds to the magnitude of the gradient of the fundamental solution to the $n$-dimensional Laplace equation (i.e., a generalized inverse-power force field). The triple integral ($n = 3$, $\alpha = 2$)

$$\iiint_{[-1,1]^3} \frac{1}{(x-e_1)^2 + (y-e_2)^2 + (z-e_3)^2 + c^2} \, \mathrm{d}x \, \mathrm{d}y \, \mathrm{d}z \tag{3.2}$$

features a regularised $\mathcal{O}(r^{-2})$ kernel, representing an inverse-square force field prevalent in 3D gravitational and electrostatic interactions [34, 31]. The quadruple integral




(a) $c = 10^{-3}$, centred (b) $c = 10^{-4}$, centred (c) $c = 10^{-5}$, centred (d) $c = 10^{-6}$, centred




(e) $c = 10^{-3}$, near edge (f) $c = 10^{-4}$, near edge (g) $c = 10^{-5}$, near edge (h) $c = 10^{-6}$, near edge

Fig. 3: Errors with and without sinh transformation, $n = 2$. Top row: source centred ($e_1 = e_2 = 0$). Bottom row: source near boundary ($e_1 = e_2$ as indicated).

($n = 4$, $\alpha = 3$)

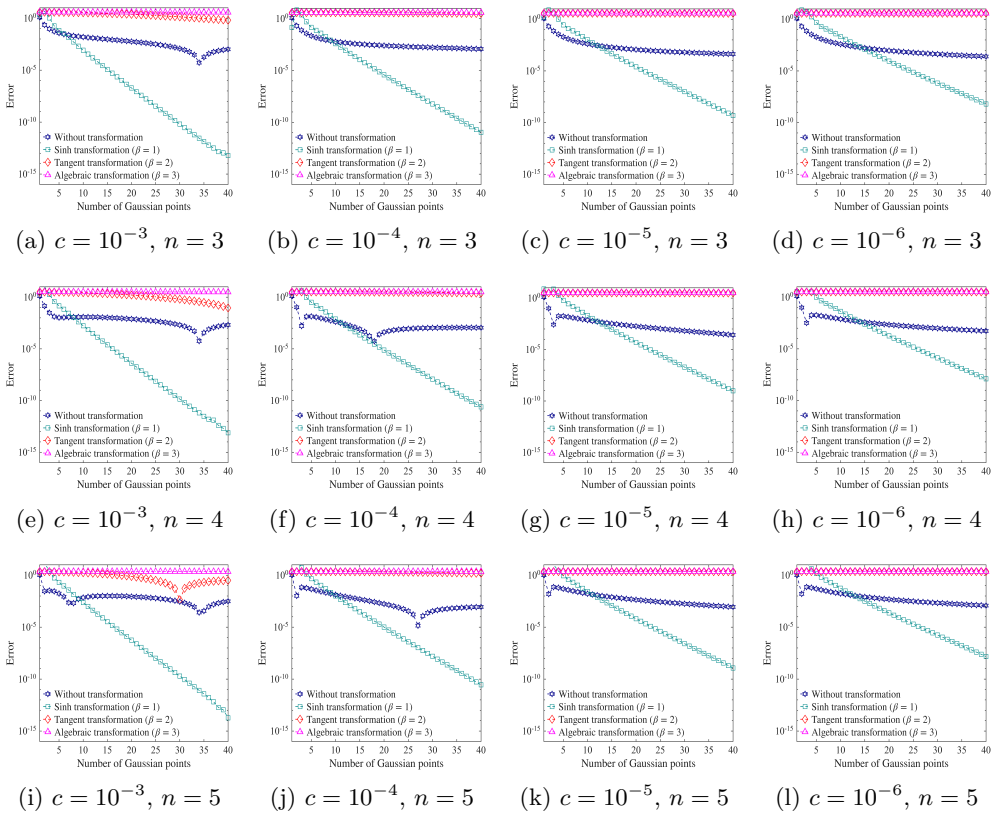
(3.3)
$$\iiiint_{[-1,1]^4} \frac{1}{\left((x-e_1)^2 + (y-e_2)^2 + (z-e_3)^2 + (w-e_4)^2 + c^2\right)^{3/2}} \,\mathrm{d}x\,\mathrm{d}y\,\mathrm{d}z\,\mathrm{d}w$$

extends this hierarchy to four dimensions with an $\mathcal{O}(r^{-3})$ kernel. Such high-dimensional potentials arise frequently in 4D potential theory [37] and the evaluation of inverse multiquadric radial basis functions in meshless approximation methods. The quintuple integral ($n = 5$, $\alpha = 4$)

(3.4)
$$\iiiint_{[-1,1]^5} \frac{1}{\left((x-e_1)^2 + \cdots + (v-e_5)^2 + c^2\right)^2} \,\mathrm{d}x\,\mathrm{d}y\,\mathrm{d}z\,\mathrm{d}w\,\mathrm{d}v$$

further generalizes the force field to five dimensions with an $\mathcal{O}(r^{-4})$ kernel. Such integrals are natively encountered when spatial models are augmented with multidimensional parameter spaces, such as in high-dimensional uncertainty quantification [19]. Figure 4 compares the sinh ($\beta = 1$), tangent ($\beta = 2$), and algebraic ($\beta = 3$) transformations against direct Gauss–Legendre quadrature. In all cases, the sinh transformation yields exponential convergence; the tangent and algebraic transformations perform worse than direct Gauss–Legendre, corroborating the theoretical prediction of Section 2.5. Robust exponential convergence persists up to $n = 5$.

**4. Significance for variational discretisations.** The preceding sections analysed the quadrature error of an individual integral. In this section, we show the accurate evaluation of singular and nearly singular integrals is critical for the overall accuracy of numerical methods based on variational formulations. The framework




(a) $c = 10^{-3}$, $n = 3$ (b) $c = 10^{-4}$, $n = 3$ (c) $c = 10^{-5}$, $n = 3$ (d) $c = 10^{-6}$, $n = 3$

(e) $c = 10^{-3}$, $n = 4$ (f) $c = 10^{-4}$, $n = 4$ (g) $c = 10^{-5}$, $n = 4$ (h) $c = 10^{-6}$, $n = 4$

(i) $c = 10^{-3}$, $n = 5$ (j) $c = 10^{-4}$, $n = 5$ (k) $c = 10^{-5}$, $n = 5$ (l) $c = 10^{-6}$, $n = 5$

Fig. 4: Errors for different hypergeometric transformations, $n = 3, 4, 5$. Rows from top to bottom: $n = 3$, $n = 4$, $n = 5$. The sinh transformation ($\beta = 1$) consistently outperforms direct Gauss–Legendre and the $\beta = 2, 3$ alternatives.

presented here applies to any discretisation method that relies on numerical integration of weak forms, including finite element, boundary element, and enriched Galerkin methods.

**4.1. Strang's first lemma and the consistency error.** Consider an abstract variational problem: find $u \in V$ such that

$$a(u, w) = l(w), \quad \forall w \in V, \tag{4.1}$$

where $V$ is an appropriate Hilbert space, $a(\cdot, \cdot) : V \times V \to \mathbb{R}$ is a bounded and coercive bilinear form, and $l(\cdot) : V \to \mathbb{R}$ is a bounded linear functional. When the integrals defining $a$ and $l$ involve singular or nearly singular kernels, they cannot be evaluated exactly and must be approximated by numerical quadrature. Let $\mathcal{T}_h$ denote a regular partition of the domain into elements $K$, and let $Q_K$ be a quadrature rule on $K$ with weights $\omega_{q,K}$ and abscissae $\boldsymbol{x}_{q,K}$. The exact bilinear and linear forms,

$$a(v_h, w_h) = \sum_{K \in \mathcal{T}_h} \int_K \mathcal{K}_a(v_h, w_h; \boldsymbol{x}) \, \mathrm{d}\boldsymbol{x}, \qquad l(w_h) = \sum_{K \in \mathcal{T}_h} \int_K \mathcal{K}_l(w_h; \boldsymbol{x}) \, \mathrm{d}\boldsymbol{x}, \tag{4.2}$$

are replaced by their approximate counterparts

(4.3)
$$a_h(v_h, w_h) = \sum_{K\in\mathcal{T}_h} \sum_{q=1}^{N_q} \omega_{q,K}\, \mathcal{K}_a(v_h, w_h; \boldsymbol{x}_{q,K}), l_h(w_h) = \sum_{K\in\mathcal{T}_h} \sum_{q=1}^{N_q} \omega_{q,K}\, \mathcal{K}_l(w_h; \boldsymbol{x}_{q,K}).$$

The fully discrete problem is then: find $\tilde{u}_h \in V_h$ such that $a_h(\tilde{u}_h, w_h) = l_h(w_h)$ for all $w_h \in V_h$. Strang's first lemma [52] provides an upper bound for the total error between $\tilde{u}_h$ and the exact solution $u$:

(4.4)
$$\|u-\tilde{u}_h\|_V \le C_0 \inf_{v_h\in V_h} \Big( \|u-v_h\|_V + \sup_{w_h\in V_h} \frac{|a(v_h, w_h) - a_h(v_h, w_h)|}{\|w_h\|_V} \Big) + C_0 \sup_{w_h\in V_h} \frac{|l(w_h) - l_h(w_h)|}{\|w_h\|_V},$$

where $C_0 = \max(1 + M/\tilde{\alpha},\, 1/\tilde{\alpha})$ depends only on the continuity constant $M$ and the coercivity constant $\tilde{\alpha}$ of $a(\cdot,\cdot)$. The first term in the infimum is the best approximation error, governed solely by the approximation power of $V_h$. The remaining terms are consistency errors induced purely by numerical quadrature.

Let $E_K(\phi) = \int_K \phi \,\mathrm{d}\boldsymbol{x} - Q_K(\phi)$ denote the local quadrature error functional on element $K$. The global consistency errors are bounded by the sum of local errors:

(4.5)
$$\begin{aligned} |a(v_h, w_h) - a_h(v_h, w_h)| &\le \sum_{K\in\mathcal{T}_h} |E_K(\mathcal{K}_a(v_h, w_h))|, \\ |l(w_h) - l_h(w_h)| &\le \sum_{K\in\mathcal{T}_h} |E_K(\mathcal{K}_l(w_h))|. \end{aligned}$$

**4.2. Effect of quadrature quality on the consistency error.** When the kernel in $\mathcal{K}_a$ or $\mathcal{K}_l$ is singular, standard Gauss–Legendre quadrature applied without transformation converges only algebraically. For an $n$-dimensional integral, the local quadrature error satisfies

(4.6)
$$|E_K(\phi)| \le \sum_{j=1}^{n} C_j m_j^{-q_j},$$

where $q_j > 0$ are dimension-dependent algebraic rates and $m_j$ is the number of quadrature points in the $j$-th direction. In the case of nearly singular integrals, the situation is more subtle: exponential convergence is formally present, but the Bernstein ellipse parameter $\rho_j$ approaches unity as $r_0 \to 0$, so that the exponential rate $\ln \rho_j$ tends to zero. In both cases, the consistency error may dominate the best approximation error, preventing the fully discrete solution from attaining the optimal convergence rate predicted by Céa's lemma.

The variable transformations developed in Section 2.1 change the character of the quadrature error. For singular integrals, the Duffy transformation cancels the $1/r^\alpha$ singularity, converting the integrand to a form that is regular (or mildly singular) in the radial direction. For nearly singular integrals, the sinh transformation regularises the near-singularity so that the transformed integrand is substantially smoother.

Bounding the consistency error in Equation (4.4) requires evaluating the quadrature error of the product integrands $\mathcal{K}_a$ and $\mathcal{K}_l$. To isolate the test function norm $\|w_h\|_V$ from the supremum, the maximum modulus of the transformed integrands on the complex Bernstein ellipse $E_\rho$ is evaluated. By invoking a stable decomposition of the enriched space and applying Bernstein's inequality for polynomials on ellipses to the standard components, the test function norm factors out (see Appendix B).

Substituting the resulting local bounds into the Strang estimate (Equation (4.4)) yields the total error bound after transformation (see Appendix B for the complete derivation):

$$\|u-\tilde{u}_h\|_V \le C_0 \inf_{v_h\in V_h}\|u-v_h\|_V + \tilde{C}\sum_{K\in\mathcal{T}_h}\sum_{j=1}^{n}\big(\rho_j^{p-1}+M_\psi(\rho_j)\big)\rho_j^{-2m_j}, \tag{4.7}$$

where $p$ is the polynomial degree of the standard finite element space, and $M_\psi(\rho_j)$ bounds the analytic continuation of the regularised enrichment function on $E_{\rho_j}$.

Because the variable transformations guarantee $\rho_j > 1$, the consistency terms decay exponentially at an asymptotic rate of $\mathcal{O}(\rho_j^{-(2m_j-p+1)})$. Provided the quadrature order $m_j$ is chosen sufficiently large to overcome the polynomial growth factor $\rho_j^{p-1}$, the consistency error vanishes at a rate faster than the approximation error $\inf_{v_h\in V_h}\|u-v_h\|_V$. The fully discrete solution therefore recovers the optimal asymptotic convergence rate dictated solely by the approximation properties of the enriched space $V_h^{\mathrm{enr}}$.

**4.3. Numerical illustration.** To illustrate the effect of quadrature quality on the total discretisation error, we consider a one-dimensional problem whose exact solution possesses a severe near-singularity:

$$-u''(x)=f(x),\quad x\in(0,1),\qquad u(0)=0,\ \ u(1)=\arctan\left(\frac{1}{\epsilon}\right), \tag{4.8}$$

with the source term $f(x)=\frac{2\epsilon x}{(x^2+\epsilon^2)^2}$ and $\epsilon \ll 1$ acting as the near-singularity parameter. The exact solution is $u_{\mathrm{ex}}(x)=\arctan\left(\frac{x}{\epsilon}\right)$.

The gradient $u'_{\mathrm{ex}}(x)=\frac{\epsilon}{x^2+\epsilon^2}$ exhibits a sharp peak at $x=0$, causing standard piecewise-linear finite elements to converge at suboptimal rates. Motivated by the known structure of the near-singularity, the trial space is augmented by the global enrichment function

$$\psi(x)=\arctan\left(\frac{x}{\epsilon}\right)-\arctan\left(\frac{1}{\epsilon}\right)x,\qquad \psi(0)=0,\ \ \psi(1)=0, \tag{4.9}$$

which exactly reproduces the singular behaviour of $u_{\mathrm{ex}}$ while satisfying homogeneous boundary conditions. The discrete solution is sought in the enriched space $V_h^{\mathrm{enr}}=V_h\oplus \mathrm{span}\{\psi\}$, where $V_h$ is the standard piecewise-linear space. The enrichment introduces the derivative

$$\psi'(x)=\frac{\epsilon}{\epsilon^2+x^2}-\arctan\left(\frac{1}{\epsilon}\right). \tag{4.10}$$

The integrand exhibits a near-singularity at $x=0$. To regularise this integral, we introduce the sinh transformation $x=\epsilon\sinh(t)$. To investigate the quadrature-induced consistency error independently of the approximation error, we define computable consistency error indicators. Following the stable decomposition and inverse estimate bounds derived in Appendix B, the global suprema over the test space in Strang's first lemma are tracked by separating the local quadrature errors of the bilinear and linear forms. We define the bilinear consistency indicator $\eta_{c,a}$ and the linear

consistency indicator $\eta_{c,l}$ as:

$$\eta_{c,a} = \sum_{K\in\mathcal{T}_h} h_K^{1/2}\Big(|E_K(u'_{\text{ex}})| + |E_K(u'_{\text{ex}}\psi')|\Big), \tag{4.11}$$

$$\eta_{c,l} = \sum_{K\in\mathcal{T}_h} h_K^{1/2}\Big(|E_K(f)| + |E_K(f\psi)|\Big), \tag{4.12}$$

where $E_K(\cdot)$ denotes the local quadrature error functional, and $h_K^{1/2}$ is the geometric scaling factor arising from the 1D inverse estimate.

Figure 5 displays the total error $\|u_{\text{ex}} - \tilde{u}_h\|_{H^1}$ and the total consistency error $\eta_c$ (as well as its components) as functions of the number of Gauss points per element, for mesh sizes $h \in \{1/8, 1/16, 1/32, 1/64\}$ and near-singularity strengths $\epsilon \in \{10^{-4}, 10^{-5}, 10^{-6}\}$. As depicted, when direct Gauss–Legendre quadrature is applied without transformation, the consistency error decays at an arbitrarily slow algebraic rate. Consequently, the total discretisation error plateaus prematurely, completely dominated by the quadrature error rather than the mesh size $h$.

Upon applying the sinh transformation, the consistency error transitions to an exponential convergence regime. The observed convergence rates associated with the bilinear and linear forms are comparable, as demonstrated by the analysis in Appendix B. Because the consistency error decreases rapidly, the total error strictly follows the theoretical approximation error down to the machine precision limits. Furthermore, as the near-singularity severity increases (i.e., smaller $\epsilon$), the absolute magnitude of the untransformed consistency error grows substantially, confirming the absolute necessity of the transformation to maintain robustness in the numerical scheme.

**5. Computational cost and implementation.**

*Time complexity.* The sinh transformation is employed in both the Duffy domain and the physical Cartesian domain for arbitrary dimensions. The only difference is the number of sub-integrals: $2n!$ in the Duffy domain compared to $2^n$ in the physical domain. After applying the sinh transformation to each dimension, the total quadrature error is

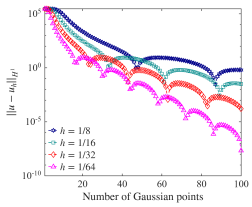
$$|E_{\text{total}}| = \sum_{j=1}^{n} C_j \rho_j^{-2m_j}, \tag{5.1}$$

where $\rho_j \gg 1$ is the Bernstein parameter for the $j$-th dimension. To obtain a simple closed-form estimate, we distribute the total error budget $\epsilon$ uniformly across all $n$ dimensions, i.e. $C_j\rho_j^{-2m_j} \le \epsilon/n$ for each $j$. This uniform allocation assumes that the dimension-dependent constants $C_j$ and the Bernstein parameters $\rho_j$ are of comparable magnitude across directions; when some directions carry substantially weaker near-singularities (i.e. larger $\rho_j$), the uniform distribution can be conservative. Solving for $m_j$ under the uniform assumption yields

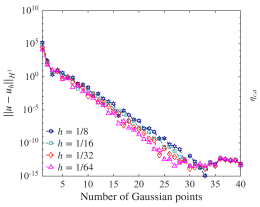
$$m_j \approx \frac{\ln(nC_j/\epsilon)}{2\ln(\rho_j)}. \tag{5.2}$$

The total number of tensor-product nodes is

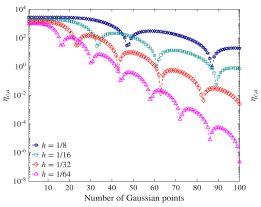
$$N_{\text{total}} = \prod_{j=1}^{n} \frac{\ln(nC_j/\epsilon)}{2\ln(\rho_j)}. \tag{5.3}$$



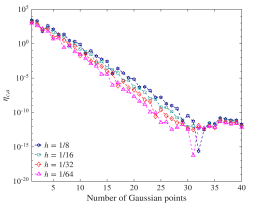

(a) Total error, no trans. ($\epsilon = 10^{-4}$)



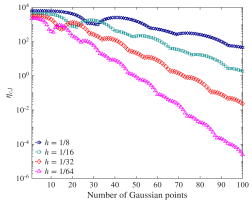

(b) Total error, with trans. ($\epsilon = 10^{-4}$)



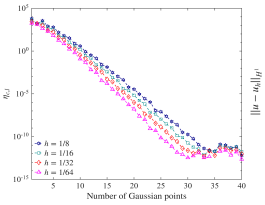

(c) Bilinear cons., no trans. ($\epsilon = 10^{-4}$)



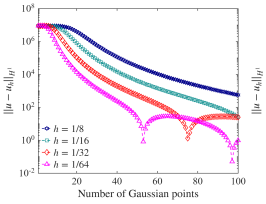

(d) Bilinear cons., with trans. ($\epsilon = 10^{-4}$)



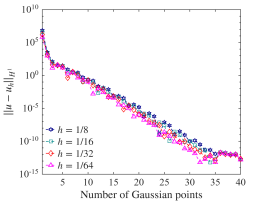

(e) Linear cons., no trans. ($\epsilon = 10^{-4}$)



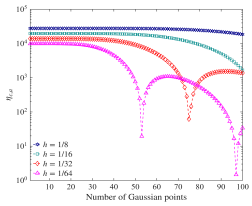

(f) Linear cons., with trans. ($\epsilon = 10^{-4}$)



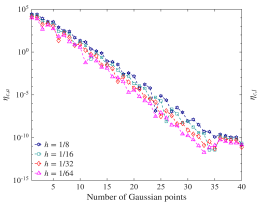

(g) Total error, no trans. ($\epsilon = 10^{-5}$)



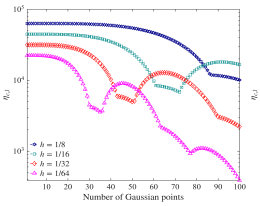

(h) Total error, with trans. ($\epsilon = 10^{-5}$)



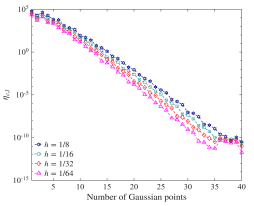

(i) Bilinear cons., no trans. ($\epsilon = 10^{-5}$)



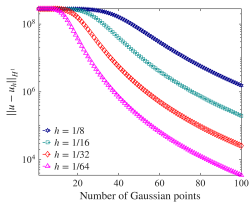

(j) Bilinear cons., with trans. ($\epsilon = 10^{-5}$)



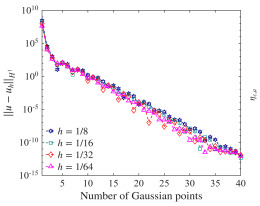

(k) Linear cons., no trans. ($\epsilon = 10^{-5}$)



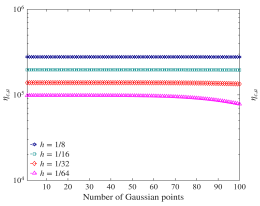

(l) Linear cons., with trans. ($\epsilon = 10^{-5}$)



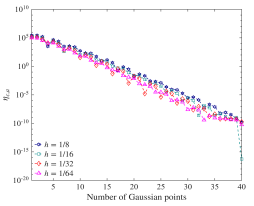

(m) Total error, no trans. ($\epsilon = 10^{-6}$)



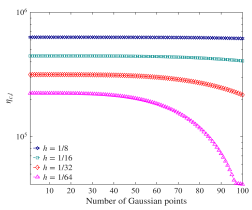

(n) Total error, with trans. ($\epsilon = 10^{-6}$)



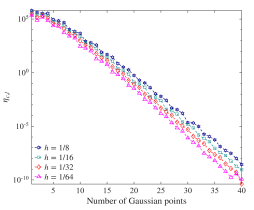

(o) Bilinear cons., no trans. ($\epsilon = 10^{-6}$)




(p) Bilinear cons., with trans. ($\epsilon = 10^{-6}$)



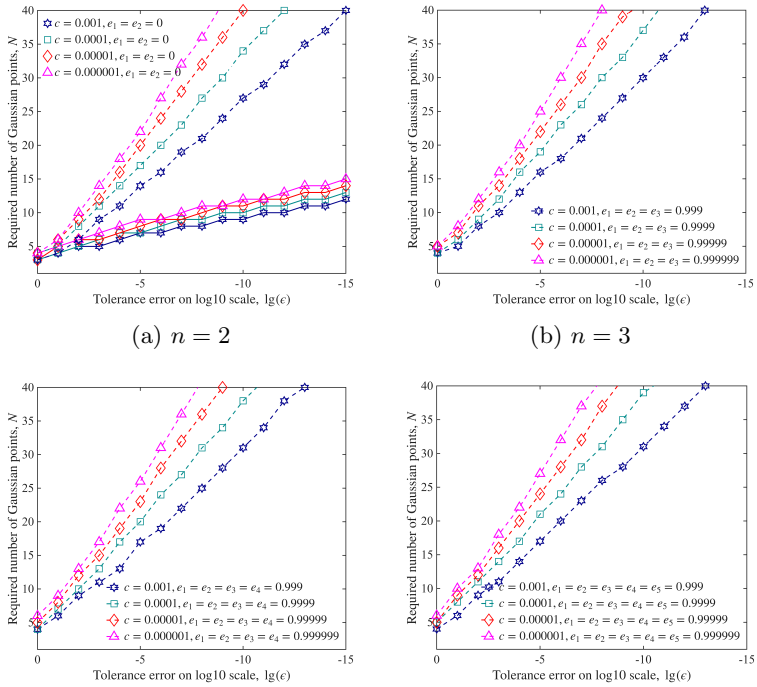

(q) Linear cons., no trans. ($\epsilon = 10^{-6}$)




(r) Linear cons., with trans. ($\epsilon = 10^{-6}$)

Fig. 5: Total error $\|u_{\text{ex}} - \tilde{u}_h\|_{H^1}$ and consistency error $\eta_c$ versus the number of Gauss points per element, evaluated for increasingly severe nearly singular parameters $\epsilon \in \{10^{-4}, 10^{-5}, 10^{-6}\}$.

Complexity grows exponentially with $n$ but is anisotropic: dimensions with weaker near-singularities require fewer nodes. Figure 6 illustrates the time complexity for $n = 2, \ldots, 5$.




(a) $n = 2$ (b) $n = 3$

(c) $n = 4$ (d) $n = 5$

Fig. 6: Required number of Gaussian points to achieve a target error tolerance for $n = 2, \ldots, 5$. In the 2D case $n = 2$, the solid and dashed lines correspond to results computed in the Duffy and physical domains, respectively.

*Space complexity.* The storage requirement scales linearly with the total number of quadrature points:

$$S_{\text{total}} \sim \mathcal{O}\Big(\prod_{j=1}^{n} m_j\Big) = \mathcal{O}\Big(\prod_{j=1}^{n} \frac{\ln(nC_j/\epsilon)}{2\ln(\rho_j)}\Big). \tag{5.4}$$

*General algorithm.* Based on the preceding analysis, Algorithm 5.1 summarises the complete procedure for evaluating singular integrals with $n \leq 2$ and nearly singular integrals in arbitrary dimensions. For the singular case, the Duffy transformation is applied to cancel the $1/r^{\alpha}$ singularity ($\alpha < n$ required), followed by a sinh transformation on $\theta_2$ to handle any angular near-singularity. The nearly singular case branches on dimension: for $n \leq 2$, the Duffy domain is used with independent sinh transformations on $\theta_1$ and $\theta_2$; for $n > 2$, the physical domain is used with independent sinh transformations on each coordinate direction.

**6. Concluding remarks.** We have developed a unified framework for the numerical evaluation of singular and nearly singular integrals based on variable trans-

**Algorithm 5.1** Evaluation of singular and nearly singular integrals.

**Input:** Source $\boldsymbol{x}_s$, element $\mathbf{D}$, integrand $f(\boldsymbol{x})/\|\boldsymbol{x}-\boldsymbol{x}_s\|^\alpha$, quadrature order $m$.
**Output:** Integral value $I$.

**if** $\boldsymbol{x}_s$ is on the element $\mathbf{D}$ (singular case) **then**
  Let $\boldsymbol{x}_0 = \boldsymbol{x}_s$. Find local coordinates $\bar{\boldsymbol{x}}_0$.
  Subdivide $\mathbf{D}$ into $2 \cdot n!$ sub-simplices $\mathbf{D}_i$ sharing $\bar{\boldsymbol{x}}_0$.
  Initialise $I \leftarrow 0$.
  **for** each sub-simplex $\mathbf{D}_i$ **do**
    Apply the $n$-dimensional Duffy transformation, mapping $\mathbf{D}_i \to [0,1]^n$.
    Compute geometric coefficients $t_1, t_2, t_3$ from the simplex vertices.
    Apply sinh transformation $\theta_2 = \theta_2(\Theta_2)$ to regularise the angular variable.
    Evaluate $I_i$ using $m$-point Gauss–Legendre quadrature in $(\theta_1, \Theta_2)$.
    $I \leftarrow I + I_i$.
  **end for**
**else** {Nearly singular case}
  Find projection $\boldsymbol{x}_0 \in \mathbf{D}$ nearest to $\boldsymbol{x}_s$; compute $r_0 = \|\boldsymbol{x}_0 - \boldsymbol{x}_s\|$.
  Find local coordinates $\bar{\boldsymbol{x}}_0$ of $\boldsymbol{x}_0$.
  **if** $n \leq 2$ **then**
    Subdivide $\mathbf{D}$ into sub-regions $\mathbf{D}_i$ in the Duffy domain.
    **for** each sub-region $\mathbf{D}_i$ **do**
      Apply Duffy transformation. Compute geometric coefficients.
      Apply sinh transformation to $\theta_1$ and $\theta_2$.
      Evaluate $I_i$ with Gauss–Legendre in $(\Theta_1, \Theta_2)$.
    **end for**
  **else**
    Subdivide $\mathbf{D}$ into $2^n$ hyper-rectangles in the physical domain.
    **for** each hyper-rectangle **do**
      Compute $c_k = \mathbf{S}^{(k)} \cdot \mathbf{S}^{(k)}$ for each direction $k = 1, \ldots, n$.
      For each direction $k$, compute sinh transformation parameters $\Theta_k(a_k)$, $\Theta_k(b_k)$.
      Apply sinh transformation $\xi^{(k)} = \xi^{(k)}(\Theta_k)$ to each direction.
      Evaluate $I_i$ with $m$-point Gauss–Legendre in $(\Theta_1, \ldots, \Theta_n)$.
    **end for**
  **end if**
  $I \leftarrow \sum_i I_i$.
**end if**
**return** $I$.

formations. The principal findings are:

1. Singular integrals. The Duffy transformation provides a valid method in any dimension $n$: the Jacobian cancels the radial singularity when $\alpha < n$, yielding exponential convergence in the radial direction for $\alpha \leq n-1$ and algebraic convergence of order $2(n-\alpha)$ for $n-1 < \alpha < n$. For well-shaped simplices, angular convergence is exponential regardless of $n$. For distorted simplices when $n > 2$, the angular variables couple through $c_2$, creating an $(n-2)$-dimensional near-singular manifold that degrades the convergence rate. This is a robustness limitation of the Duffy method.
2. Nearly singular integrals. The Duffy domain admits a complete separable

treatment only for $n = 2$, where independent sinh transformations on $\theta_1$ and $\theta_2$ suffice. For $n > 2$, the same geometric obstruction that affects distorted singular simplices becomes fatal: the near-singular manifold has dimension $\geq 1$ and cannot be resolved by a tensor-product rule. Switching to the physical domain resolves this obstruction: the near-singularities align with the coordinate axes, and the sinh transformation applied independently to each dimension yields exponential convergence for any $n$.

3. Transformation selection. A Bernstein-ellipse convergence analysis proves that among the three closed-form members of the Gauss hypergeometric family, only the sinh transformation ($\beta = 1$) consistently improves convergence. The tangent ($\beta = 2$) and algebraic ($\beta = 3$) transformations introduce secondary near-singularities through their Jacobians and are ineffective.
4. Variational discretisations. A Strang-lemma analysis demonstrates that the improved quadrature accuracy directly translates to optimal asymptotic convergence rates. The consistency error decays exponentially, eliminating the quadrature bottleneck and allowing the discrete solution to achieve the rate dictated by approximation theory.

Future work may address the extension to curved elements with rigorous treatment of cross-terms in the physical domain, adaptive transformation strategies, and the coupling with sparse-grid quadrature to mitigate the exponential growth of tensor-product cost in very high dimensions.

## Appendix A. Convergence of the tangent and algebraic transformations.

**A.1. Tangent transformation ($\beta = 2$).** The upper integration limit after the tangent transformation is

$$\Theta_1 = \frac{\arctan(\sqrt{c}/r_0)}{\sqrt{c}\, r_0} \xrightarrow{r_0 \to 0} \frac{\pi}{2\sqrt{c}\, r_0}. \tag{A.1}$$

The Jacobian $\sec^2(r_0\sqrt{c}\,\Theta)$ has singularities at $r_0\sqrt{c}\,\Theta_s = \pi/2 + k\pi$. Mapping to the $p$-domain:

$$p_s^{(\beta=2)} = \frac{2\Theta_s}{\Theta_1} - 1 = \frac{\pi}{\arctan(\sqrt{c}/r_0)} - 1 \xrightarrow{r_0 \to 0} \frac{\pi}{\pi/2} - 1 = 1. \tag{A.2}$$

The Bernstein parameter tends to unity and the convergence is arbitrarily slow.

**A.2. Algebraic transformation ($\beta = 3$).** The upper limit is

$$\Theta_1 = \frac{1}{r_0^2\sqrt{r_0^2 + c}} \xrightarrow{r_0 \to 0} \frac{1}{r_0^2\sqrt{c}}. \tag{A.3}$$

The Jacobian $(1 - cr_0^4\Theta^2)^{-3/2}$ has singularities at $\Theta_s = \pm 1/(r_0^2\sqrt{c})$. Mapping to the $p$-domain gives $p_s^{(\beta=3)} \approx 1$, again collapsing the Bernstein parameter to unity.

**A.3. Behaviour in the physical domain.** The preceding analysis was conducted for a single variable in the Duffy domain. We now verify that the same qualitative conclusions hold in the physical Cartesian domain, where the sinh transformation is applied independently to each coordinate direction. The analysis is presented for the first coordinate $\xi^{(1)} \equiv x_1$; the treatment of the remaining coordinates is identical.

**A.3.1. Sinh transformation ($\beta = 1$) in the physical domain.** After applying the sinh transformation to $x_1$ in Eq. (2.20) with $\alpha = 1$, the sub-integral becomes

$$I_l = \int_{-1}^{1}\int_{a_2}^{b_2}\cdots\int_{a_n}^{b_n} \frac{f(\mathbf{x})}{\left(r_0^2 + \sum_{j=1}^{n}\sum_{k=1}^{n}\mathbf{S}^{(j)}\cdot\mathbf{S}^{(k)}\,\boldsymbol{\xi}^{(j)}\boldsymbol{\xi}^{(k)}\right)^{1/2}} \frac{\mathrm{d}x_1}{\mathrm{d}\theta_1}\,\mathrm{d}\theta_1\,\mathrm{d}x_2\cdots\mathrm{d}x_n. \tag{A.4}$$

The Jacobian of the sinh transformation in the physical domain takes the form

$$\frac{\mathrm{d}x_1}{\mathrm{d}\theta_1} = \frac{r_0 k_1}{\sqrt{c_1}}\cosh(k_1\theta_1 + k_2), \tag{A.5}$$

with the coefficients

$$\begin{aligned} k_1 &= \frac{1}{2}\operatorname{arcsinh}\Big(\frac{\sqrt{c_1}(b_1 - x_{0,1})}{r_0}\Big) - \frac{1}{2}\operatorname{arcsinh}\Big(\frac{\sqrt{c_1}(a_1 - x_{0,1})}{r_0}\Big), \\ k_2 &= \frac{1}{2}\operatorname{arcsinh}\Big(\frac{\sqrt{c_1}(b_1 - x_{0,1})}{r_0}\Big) + \frac{1}{2}\operatorname{arcsinh}\Big(\frac{\sqrt{c_1}(a_1 - x_{0,1})}{r_0}\Big), \end{aligned} \tag{A.6}$$

where $x_{0,i}$ denotes the $i$-th component of $\mathbf{x}_0$, $c_1 = \mathbf{S}^{(1)}\cdot\mathbf{S}^{(1)}$. The cosh function has its nearest singularity in the complex $\theta_1$-plane at $\theta_1 = i\pi/(2k_1) - k_2/k_1$. Because $k_1$ and $k_2$ involve $\operatorname{arcsinh}(\cdot/r_0)$, they grow only logarithmically as $r_0 \to 0$, pushing the singularity away from the real axis. The transformed integrand therefore exhibits no near-singular behaviour, and Gauss–Legendre quadrature converges rapidly.

**A.3.2. Tangent transformation ($\beta = 2$) in the physical domain.** For $\alpha = 2$, the tangent transformation is applied. After transformation, the Jacobian becomes

$$\frac{\mathrm{d}x_1}{\mathrm{d}\Theta_1} = \frac{r_0 k_1}{\sqrt{c_1}}\sec^2(k_1\Theta_1 + k_2), \tag{A.7}$$

where now

$$\begin{aligned} k_1 &= \frac{1}{2}\arctan\Big(\frac{\sqrt{c_1}(b_1 - x_{0,1})}{r_0}\Big) - \frac{1}{2}\arctan\Big(\frac{\sqrt{c_1}(a_1 - x_{0,1})}{r_0}\Big), \\ k_2 &= \frac{1}{2}\arctan\Big(\frac{\sqrt{c_1}(b_1 - x_{0,1})}{r_0}\Big) + \frac{1}{2}\arctan\Big(\frac{\sqrt{c_1}(a_1 - x_{0,1})}{r_0}\Big). \end{aligned} \tag{A.8}$$

The Jacobian (A.7) has singularities at $\Theta_1 = (\pm\pi - 2k_2)/(2k_1)$. Mapping these to the standard interval $[-1, 1]$ via $p = 2(\Theta_1 - \Theta_1(a_1))/(\Theta_1(b_1) - \Theta_1(a_1)) - 1$ yields

$$p_s = \frac{\pm\pi - \arctan\big(\frac{\sqrt{c_1}(b_1 - x_{0,1})}{r_0}\big) - \arctan\big(\frac{\sqrt{c_1}(a_1 - x_{0,1})}{r_0}\big)}{\arctan\big(\frac{\sqrt{c_1}(b_1 - x_{0,1})}{r_0}\big) - \arctan\big(\frac{\sqrt{c_1}(a_1 - x_{0,1})}{r_0}\big)}. \tag{A.9}$$

When the projection point lies on the isoparametric domain boundary, i.e. $b_1 = x_{0,1}$ or $a_1 = x_{0,1}$, the corresponding arctan terms vanish, and $p_s$ approaches $\pm 1$. The Bernstein ellipse parameter therefore collapses to unity when the source projects onto the element boundary, which is the most critical case in practice.

**A.3.3. Algebraic transformation ($\beta = 3$) in the physical domain.** For $\alpha = 3$, the algebraic transformation is applied. The Jacobian is

$$\frac{\mathrm{d}x_1}{\mathrm{d}\Theta_1} = \frac{r_0^3}{(1 - c_1 r_0^4 \Theta_1^2)^{3/2}}, \tag{A.10}$$

with singularities at $\Theta_1 = \pm 1/(r_0^2\sqrt{c_1})$. The integration limits are

$$\Theta_1(a_1) = \frac{a_1 - x_{0,1}}{r_0^2\sqrt{r_0^2 + c_1(a_1 - x_{0,1})^2}}, \qquad \Theta_1(b_1) = \frac{b_1 - x_{0,1}}{r_0^2\sqrt{r_0^2 + c_1(b_1 - x_{0,1})^2}}. \tag{A.11}$$

Mapping the singularities to $[-1, 1]$ gives

$$p_s = \frac{\pm 2 - \frac{\sqrt{c_1}(a_1 - x_{0,1})}{\sqrt{r_0^2 + c_1(a_1 - x_{0,1})^2}} - \frac{\sqrt{c_1}(b_1 - x_{0,1})}{\sqrt{r_0^2 + c_1(b_1 - x_{0,1})^2}}}{\frac{\sqrt{c_1}(a_1 - x_{0,1})}{\sqrt{r_0^2 + c_1(a_1 - x_{0,1})^2}} - \frac{\sqrt{c_1}(b_1 - x_{0,1})}{\sqrt{r_0^2 + c_1(b_1 - x_{0,1})^2}}}. \tag{A.12}$$

As $r_0 \to 0$, the terms $\frac{\sqrt{c_1}(a_1 - x_{0,1})}{\sqrt{r_0^2 + c_1(a_1 - x_{0,1})^2}}$ or $\frac{\sqrt{c_1}(b_1 - x_{0,1})}{\sqrt{r_0^2 + c_1(b_1 - x_{0,1})^2}}$ approach $\pm 1$. Consequently, the numerator and denominator tend to values that drive $p_s$ to $\pm 1$, collapsing the Bernstein ellipse parameter to unity.

In summary, the physical-domain analysis confirms the conclusions drawn in the Duffy domain. For $\beta = 1$, the logarithmic growth of arcsinh pushes complex singularities away from the real axis, preserving exponential convergence. For $\beta = 2$ and $\beta = 3$, the Jacobian singularities map to $p_s = \pm 1$ as $r_0 \to 0$, collapsing the Bernstein parameter to unity. The sinh transformation is therefore uniquely effective in the physical domain as well.

## Appendix B. Derivation of the post-transformation error bound.

We derive the bound for the total discretisation error presented in Equation 4.7. This rigorous derivation demonstrates how the normalisation $||w_h||_V$ in Strang's first lemma is absorbed into the convergence constants by analysing the quadrature error in the complex plane, avoiding the algebraic fallacies associated with factoring quadrature errors of polynomial products.

**B.1. Strang's Lemma and Stable Decomposition.** Let $I_h u \in V_h^{enr}$ be the interpolant of the exact solution $u$. Strang's first lemma bounds the total error by the approximation error plus the consistency errors arising from both the bilinear form $a(\cdot, \cdot)$ and the linear form $l(\cdot)$:

$$\begin{aligned} ||u - \tilde{u}_h||_V \leq C_0 \inf_{v_h \in V_h} ||u - v_h||_V + C_0 \sup_{w_h \in V_h} \frac{|a(I_h u, w_h) - a_h(I_h u, w_h)|}{||w_h||_V} \\ + C_0 \sup_{w_h \in V_h} \frac{|l(w_h) - l_h(w_h)|}{||w_h||_V}. \end{aligned} \tag{B.1}$$

Given a generic element $K \in \mathcal{T}_h$, the exact local integrands for the bilinear and linear forms are denoted as $\mathcal{K}_a(I_h u, w_h; x) = \Phi_{I_h u}(x)\Psi_{a,w_h}(x)$ and $\mathcal{K}_l(w_h; x) = \Phi_l(x)\Psi_{l,w_h}(x)$, respectively. Here, $\Phi_{I_h u}$ and $\Phi_l$ capture the (nearly) singular state and source variables. The terms $\Psi_{a,w_h}$ and $\Psi_{l,w_h}$ represent the test function evaluated through the appropriate linear differential operators (e.g., the spatial gradient $\nabla w_h$ for the bilinear form, and $w_h$ for the linear form). Let $E_K(\cdot)$ denote the local

quadrature error functional such that the global consistency errors are bounded by $\sum_K |E_K(\mathcal{K}_a)|$ and $\sum_K |E_K(\mathcal{K}_l)|$.

Using the standard stable decomposition condition for enriched finite element spaces, any discrete test function $w_h \in V_h^{enr}$ can be uniquely decomposed into a standard polynomial part and an enriched part, $w_h = w_{std} + c_\psi \psi$, satisfying:

$$||w_{std}||_V \leq C_{stab}||w_h||_V, \quad |c_\psi| \leq \frac{C_{stab}}{||\psi||_V}||w_h||_V. \tag{B.2}$$

By the linearity of the quadrature error operator, the local errors split accordingly:

$$E_K(\mathcal{K}_a) = E_K(\Phi_{I_h u}\Psi_{a,w_{std}}) + c_\psi E_K(\Phi_{I_h u}\Psi_{a,\psi}), \tag{B.3}$$

$$E_K(\mathcal{K}_l) = E_K(\Phi_l \Psi_{l,w_{std}}) + c_\psi E_K(\Phi_l \Psi_{l,\psi}). \tag{B.4}$$

**B.2. Bounding the Bilinear Form Consistency Error.** After applying the appropriate variable transformation (e.g. the sinh transformation), the integration over $K$ is mapped to the reference domain $\hat{K} = [-1, 1]$. The transformed integrand is analytic in a region bounded by the Bernstein ellipse $E_\rho$ with parameter $\rho > 1$. The quadrature error for an $m$-point Gauss-Legendre rule is bounded by $|E_{\hat{K}}(F)| \leq C\frac{M(\rho)}{\rho-1}\rho^{-2m}$, where $M(\rho) = \max_{\xi \in E_\rho} |F(\xi)|$.

**Standard Component:** Given the mapped test function $\Psi_{w_{std}}$ is a polynomial of degree $p-1$, we apply the Bernstein's inequality for polynomials on ellipses, which bounds its maximum on $E_\rho$ by its real maximum:

$$\max_{\xi \in E_\rho} |\Psi_{w_{std}}(\xi)| \leq \rho^{p-1}||\Psi_{w_{std}}||_{L^\infty(\hat{K})}. \tag{B.5}$$

Mapping back to the physical element and utilising the standard finite element inverse estimate $||\Psi||_{L^\infty(K)} \leq C_{inv} h_K^{-d/2}||\Psi||_{L^2(K)}$, we obtain:

$$\max_{\xi \in E_\rho} |\Psi_{w_{std}}(\xi)| \leq \rho^{p-1} C_{inv} h_K^{-d/2}||w_{std}||_{V,K} \leq \rho^{p-1} C_{inv} C_{stab} h_K^{-d/2}||w_h||_V. \tag{B.6}$$

Incorporating the geometric Jacobian $J_K \propto h_K^d$, the quadrature bound for the standard part of the bilinear form isolates $||w_h||_V$:

$$|E_K(\Phi_{I_h u}\Psi_{w_{std}})| \leq \left[ C_{inv} C_{stab} h_K^{d/2} \left( \max_{E_\rho} |\Phi_{I_h u}| \right) \right] ||w_h||_V \frac{\rho^{p-1-2m}}{\rho - 1}. \tag{B.7}$$

**Enriched Component:** The enrichment function $\Psi_\psi$ is not a polynomial, and Bernstein's inequality does not apply. However, consider that the sinh transformation regularises the nearly singular behaviour, its analytic continuation is bounded on $E_\rho$ by a finite constant $M_\psi(\rho)$. Utilising the stable decomposition bound for $c_\psi$ from (B.2):

$$|c_\psi E_K(\Phi_{I_h u}\Psi_\psi)| \leq \left[ \frac{C_{stab}}{||\psi||_V} h_K^d \left( \max_{E_\rho} |\Phi_{I_h u}| \right) M_\psi(\rho) \right] ||w_h||_V \frac{\rho^{-2m}}{\rho - 1}. \tag{B.8}$$

**B.3. Bounding the Linear Form Consistency Error.** The linear form consistency error follows a similar analytic structure. Applying the Bernstein inequality to the standard component $\Psi_{l,w_{std}}$ bounds its maximum by the local $L^2(K)$ norm. To relate this back to the global energy norm, we invoke the global Poincaré inequality

$||w_{std}||_{L^2(\Omega)} \leq C_P||w_{std}||_V$, where $C_P$ is the Poincaré constant associated with the domain diameter. This yields:

$$|E_K(\Phi_l\Psi_{l,w_{std}})| \leq \left[C_{inv}C_{stab}C_P h_K^{d/2}\left(\max_{E_\rho}|\Phi_l|\right)\right]||w_h||_V\frac{\rho^{p-1-2m}}{\rho-1}. \tag{B.9}$$

Because $C_P$ carries the physical dimension of length, this inequality remains dimensionally consistent with the physical integral.

Similarly, the enriched component of the linear form relies on the bounded analytic continuation of the transformed source term product on $E_\rho$, denoted $M_{l,\psi}(\rho)$. Utilising the stable decomposition directly bypasses the Poincaré inequality:

$$|c_\psi E_K(\Phi_l\Psi_{l,\psi})| \leq \left[\frac{C_{stab}}{||\psi||_V}h_K^d\left(\max_{E_\rho}|\Phi_l|\right)M_{l,\psi}(\rho)\right]||w_h||_V\frac{\rho^{-2m}}{\rho-1}. \tag{B.10}$$

**B.4. Global Assembly and Optimal Convergence.** Summing the local standard and enriched bounds for both forms, the global test function norm $||w_h||_V$ can now be factored out of the local quadrature errors. Substituting into the normalised consistency terms in Strang's lemma (B.1) cancels $||w_h||_V$ entirely:

$$\sup_{w_h\in V_h}\frac{|a(I_hu,w_h)-a_h(I_hu,w_h)|}{||w_h||_V} \leq \sum_{K\in\mathcal{T}_h}\tilde{C}_{a,K}\left(\rho^{p-1}+M_\psi(\rho)\right)\rho^{-2m}, \tag{B.11}$$

$$\sup_{w_h\in V_h}\frac{|l(w_h)-l_h(w_h)|}{||w_h||_V} \leq \sum_{K\in\mathcal{T}_h}\tilde{C}_{l,K}\left(\rho^{p-1}+M_{l,\psi}(\rho)\right)\rho^{-2m}, \tag{B.12}$$

where $\tilde{C}_{a,K}$ and $\tilde{C}_{l,K}$ absorb the mesh-dependent geometric constants and the maximum moduli of $\Phi_{I_hu}$ and $\Phi_l$, respectively.

As the variable transformations guarantee $\rho > 1$, both consistency errors decay exponentially at an asymptotic rate of $\mathcal{O}(\rho^{-(2m-p+1)})$. For a sufficiently large quadrature order $m$, these consistency errors become subdominant to the best approximation error $C_0\inf_{v_h\in V_h}||u-v_h||_V$, recovering the optimal asymptotic convergence rate dictated by the enriched finite element space.

**Acknowledgments.** This work was funded by Shanghai Pujiang Program (22PJD074) and the National Natural Science Foundation of China (Grant No. 12571466).

REFERENCES

[1] L. af Klinteberg and A. H. Barnett, *Accurate quadrature of nearly singular line integrals in two and three dimensions by singularity swapping*, BIT Numerical Mathematics, 61 (2021), pp. 83–118.

[2] S. Amari and J. Bornemann, *Efficient numerical computation of singular integrals with applications to electromagnetics*, IEEE Transactions on Antennas and Propagation, 43 (1995), pp. 1343–1348.

[3] T. L. Anderson and T. L. Anderson, *Fracture mechanics: fundamentals and applications*, CRC press, 2005.

[4] K. E. Atkinson, *An introduction to numerical analysis*, John wiley & sons, 2008.

[5] G. Bao, W. Hua, J. Lai, and J. Zhang, *Singularity swapping method for nearly singular integrals based on trapezoidal rule*, SIAM Journal on Numerical Analysis, 62 (2024), pp. 974–997.

[6] A. H. Barnett, *Evaluation of layer potentials close to the boundary for laplace and helmholtz problems on analytic planar domains*, SIAM Journal on Scientific Computing, 36 (2014), pp. A427–A451.

[7] J. T. Beale and M. C. Lai, *A method for computing nearly singular integrals*, SIAM Journal on Numerical Analysis, 38 (2001), pp. 1902–1925.
[8] M. Bonnet, *Boundary Integral Equation Methods for Solids and Fluids*, Wiley, 1999.
[9] R. L. Burden and J. D. Faires, *Numerical analysis*, Brooks Cole, 1997.
[10] H. S. Carslaw and J. C. Jaeger, *Conduction of Heat in Solids*, Oxford University Press, 2nd ed., 1959.
[11] P.-C. Chao, A. Gürbüz, F. Sachs, and M. Sivaselvan, *Fully implicit spectral boundary integral computation of red blood cell flow*, Physics of Fluids, 33 (2021), p. 071909.
[12] A. Chernov and A. Reinarz, *Numerical quadrature for high-dimensional singular integrals over parallelotopes*, Computers & Mathematics with Applications, 66 (2013), pp. 1213–1231.
[13] A. Chernov and C. Schwab, *Exponential convergence of gauss–jacobi quadratures for singular integrals over simplices in arbitrary dimension*, SIAM Journal on Numerical Analysis, 50 (2012), pp. 1433–1455.
[14] B. Chi, Q. Guo, L. Zhang, W. Yuan, and Y. Zhang, *An adaptive binary-tree element subdivision method for evaluation of volume integrals with continuous or discontinuous kernels*, Engineering Analysis with Boundary Elements, 134 (2022), pp. 298–314.
[15] D. Colton and R. Kress, *Integral equation methods in scattering theory*, SIAM, 2013.
[16] M. Darbas and F. Le Louër, *Well-conditioned boundary integral formulations for high-frequency elastic scattering problems in three dimensions*, Mathematical Methods in the Applied Sciences, 38 (2015), pp. 1705–1733.
[17] P. J. Davis and P. Rabinowitz, *Methods of numerical integration*, Courier Corporation, 2007.
[18] M. G. Duffy, *Quadrature over a pyramid or cube of integrands with a singularity at a vertex*, SIAM journal on Numerical Analysis, 19 (1982), pp. 1260–1262.
[19] B. Ganapathysubramanian and N. Zabaras, *Sparse grid collocation schemes for stochastic natural convection problems*, Journal of Computational Physics, 225 (2007), pp. 652–685.
[20] T. Gerstner and M. Griebel, *Numerical integration using sparse grids*, Numerical algorithms, 18 (1998), pp. 209–232.
[21] R. D. Graglia, *On the numerical integration of the linear shape functions times the 3-d green's function or its gradient on a plane triangle*, IEEE transactions on antennas and propagation, 41 (1993), pp. 1448–1455.
[22] Y. Gu, H. Gao, W. Chen, H. Wang, and C. Zhang, *A general algorithm for evaluating nearly strong-singular (and beyond) integrals in three-dimensional boundary element analysis*, Computational Mechanics, 59 (2017), pp. 779–793.
[23] M. Guiggiani, G. Krishnasamy, T. J. Rudolphi, and F. Rizzo, *A general algorithm for the numerical solution of hypersingular boundary integral equations*, Journal of Applied mechanics, 59 (1992), pp. 604–614.
[24] Z. Han, W. Pan, C. Cheng, Z. Hu, and Z. Niu, *A semi-analytical treatment for nearly singular integrals arising in the isogeometric boundary element method-based solutions of 3d potential problems*, Computer Methods in Applied Mechanics and Engineering, 398 (2022), p. 115179.
[25] J. Hu, L. He, J. Rungamornrat, and X. Gu, *Transformation techniques for weakly and nearly singular integrals: Comparative performance and numerical implementation*, Computer Physics Communications, (2026), p. 110159.
[26] J. Hu and M. E. Mear, *A computational framework for well production simulation: Coupling steady state Darcy flow and channel flow by SGBEM–FEM*, Computer Methods in Applied Mechanics and Engineering, 399 (2022), p. 115300.
[27] J. Hu, C. G. Mood, and M. E. Mear, *An efficient computational framework for height-contained growing and intersecting hydraulic fracturing simulation via SGBEM–FEM*, Computer Methods in Applied Mechanics and Engineering, 419 (2024), p. 116653.
[28] J. W. Hutchinson, M. Mear, and J. R. Rice, *Crack paralleling an interface between dissimilar materials*, Journal of Applied Mechanics, 54 (1987), pp. 828–832.
[29] D. Huybrechs and R. Cools, *On generalized gaussian quadrature rules for singular and nearly singular integrals*, SIAM journal on numerical analysis, 47 (2009), pp. 719–739.
[30] A. Ilhan, M. Jonsson, and R. Sircar, *Singular perturbations for boundary value problems arising from exotic options*, SIAM Journal on Applied Mathematics, 64 (2004), pp. 1268–1293.
[31] J. D. Jackson, *Classical Electrodynamics*, Wiley, 3rd ed., 1999.
[32] S. Järvenpää, M. Taskinen, and P. Ylä-Oijala, *Singularity extraction technique for integral equation methods with higher order basis functions on plane triangles and tetrahedra*, International journal for numerical methods in engineering, 58 (2003), pp. 1149–1165.
[33] P. R. Johnston and D. Elliott, *A sinh transformation for evaluating nearly singular bound-*

*ary element integrals*, International journal for numerical methods in engineering, 62 (2005), pp. 564–578.
[34] O. D. Kellogg, *Foundations of potential theory*, vol. 31, Courier Corporation, 1953.
[35] R. Kleinman and P. Martin, *On single integral equations for the transmission problem of acoustics*, SIAM Journal on Applied Mathematics, 48 (1988), pp. 307–325.
[36] P. Kolm and V. Rokhlin, *Numerical quadratures for singular and hypersingular integrals*, Computers & Mathematics with Applications, 41 (2001), pp. 327–352.
[37] D. Latypov, *Evaluation of the 4-d singular and near singular potential integrals via the stokes' theorem*, Engineering Analysis with Boundary Elements, 125 (2021), pp. 201–207.
[38] M. Lenoir and N. Salles, *Evaluation of 3-d singular and nearly singular integrals in galerkin bem for thin layers*, SIAM Journal on Scientific Computing, 34 (2012), pp. A3057–A3078.
[39] Y. Liu and F. Rizzo, *A weakly singular form of the hypersingular boundary integral equation applied to 3-d acoustic wave problems*, Computer Methods in Applied Mechanics and Engineering, 96 (1992), pp. 271–287.
[40] H. Montanelli, M. Aussal, and H. Haddar, *Computing weakly singular and near-singular integrals over curved boundary elements*, SIAM Journal on Scientific Computing, 44 (2022), pp. A3728–A3753.
[41] H. Montanelli, F. Collino, and H. Haddar, *Computing singular and near-singular integrals over curved boundary elements: The strongly singular case*, SIAM Journal on Scientific Computing, 46 (2024), pp. A3756–A3778.
[42] S. Mousavi and N. Sukumar, *Generalized duffy transformation for integrating vertex singularities*, Computational Mechanics, 45 (2010), pp. 127–140.
[43] Z. Niu, W. Wendland, X. Wang, and H. Zhou, *A semi-analytical algorithm for the evaluation of the nearly singular integrals in three-dimensional boundary element methods*, Computer methods in applied mechanics and engineering, 194 (2005), pp. 1057–1074.
[44] E. Novak and K. Ritter, *High dimensional integration of smooth functions over cubes*, Numerische Mathematik, 75 (1996), pp. 79–97.
[45] M. J. Ouellette and E. Fiume, *On numerical solutions to one-dimensional integration problems with applications to linear light sources*, ACM Transactions on Graphics (TOG), 20 (2001), pp. 232–279.
[46] G. Padhi, R. Shenoi, S. Moy, and M. McCarthy, *Analytic integration of kernel shape function product integrals in the boundary element method*, Computers & Structures, 79 (2001), pp. 1325–1333.
[47] V. Rokhlin, *Rapid solution of integral equations of classical potential theory*, Journal of computational physics, 60 (1985), pp. 187–207.
[48] D. Rosen and D. E. Cormack, *The continuation approach: A general framework for the analysis and evaluation of singular and near-singular integrals*, SIAM Journal on Applied Mathematics, 55 (1995), pp. 723–762.
[49] S. A. Sauter and C. Schwab, *Boundary Element Methods*, Springer, 2011.
[50] P. Schröder, *Numerical integration for radiosity in the presence of singularities*, in 4th Eurographics Workshop on Rendering, Paris, France, 1993, pp. 177–184.
[51] C. Schwab, *Variable order composite quadrature of singular and nearly singular integrals*, Computing, 53 (1994), pp. 173–194.
[52] G. Strang, G. J. Fix, and D. Griffin, *An analysis of the finite-element method*, Prentice-Hall, 1974.
[53] S. Tlupova and J. T. Beale, *Regularized single and double layer integrals in 3d stokes flow*, Journal of Computational Physics, 386 (2019), pp. 568–584.
[54] M. S. Tong and W. C. Chew, *A novel approach for evaluating hypersingular and strongly singular surface integrals in electromagnetics*, IEEE transactions on antennas and propagation, 58 (2010), pp. 3593–3601.
[55] L. N. Trefethen, *Approximation theory and approximation practice, extended edition*, SIAM, 2019.
[56] J. L. Tsalamengas, *Quadrature rules for weakly singular, strongly singular, and hypersingular integrals in boundary integral equation methods*, Journal of Computational Physics, 303 (2015), pp. 498–513.
[57] J. L. Tsalamengas, *Gauss–jacobi quadratures for weakly, strongly, hyper-and nearly-singular integrals in boundary integral equation methods for domains with sharp edges and corners*, Journal of Computational Physics, 325 (2016), pp. 338–357.
[58] S. Vijayakumar and D. E. Cormack, *A new concept in near-singular integral evaluation: the continuation approach*, SIAM Journal on Applied Mathematics, 49 (1989), pp. 1285–1295.
[59] M. Widdicks, P. W. Duck, A. D. Andricopoulos, and D. P. Newton, *The black-scholes equation revisited: Asymptotic expansions and singular perturbations*, Mathematical Fi-

nance: An International Journal of Mathematics, Statistics and Financial Economics, 15 (2005), pp. 373–391.

[60] M. L. Williams, *Stress singularities resulting from various boundary conditions in angular corners of plates in extension*, Journal of Applied Mechanics, 19(4) (1952), pp. 526–528.

[61] S. Xiang and F. Bornemann, *On the convergence rates of gauss and clenshaw–curtis quadrature for functions of limited regularity*, SIAM journal on numerical analysis, 50 (2012), pp. 2581–2587.

[62] G. Xie, J. Zhang, Y. Dong, C. Huang, and G. Li, *An improved exponential transformation for nearly singular boundary element integrals in elasticity problems*, International Journal of Solids and Structures, 51 (2014), pp. 1322–1329.

[63] Z. Xie, L. Wang, and X. Zhao, *On exponential convergence of gegenbauer interpolation and spectral differentiation*, Mathematics of Computation, 82 (2013), pp. 1017–1036.

[64] S. A. YANG, *An investigation into integral equation methods involving nearly singular kernels for acoustic scattering*, Journal of sound and vibration, 234 (2000), pp. 225–239.

[65] W. Ye, *A new transformation technique for evaluating nearly singular integrals*, Computational Mechanics, 42 (2008), pp. 457–466.

[66] L. Ying, G. Biros, and D. Zorin, *A high-order 3d boundary integral equation solver for elliptic pdes in smooth domains*, Journal of Computational Physics, 219 (2006), pp. 247–275.

[67] B. I. Yun and P. Kim, *A new sigmoidal transformation for weakly singular integrals in the boundary element method*, SIAM Journal on Scientific Computing, 24 (2003), pp. 1203–1217.

[68] X. Zhao, L. Wang, and Z. Xie, *Sharp error bounds for jacobi expansions and gegenbauer–gauss quadrature of analytic functions*, SIAM Journal on Numerical Analysis, 51 (2013), pp. 1443–1469.

[69] H. Zheng and D. Xu, *New strategies for some issues of numerical manifold method in simulation of crack propagation*, International Journal for Numerical Methods in Engineering, 97 (2014), pp. 986–1010.